Edinburgh Research Explorer

Glycolytic oligodendrocytes maintain myelin and long-term axonal integrity

Glycolytic oligodendrocytes maintain myelin and long-term axonal integrity

Ursula Funfschilling[1], **Lotti M. Supplie**[1], **Don Mahad**[2,†], **Susann Boretius**[3], **Aiman S. Saab**[1,†], **Julia Edgar**[1], **Bastian G. Brinkmann**[1,†], **Celia M. Kassmann**[1], **Iva D. Tzvetanova**[1], **Wiebke Mobius**[1,†], **Francisca Diaz**[4], **Dies Meijer**[5], **Ueli Suter**[6], **Bernd Hamprecht**[1], **Michael W. Sereda**[1,7], **Carlos T. Moraes**[4], **Jens Frahm**[3], **Sandra Goebbels**[1], and **Klaus-Armin Nave**[1]

[1]Max Planck Institute of Experimental Medicine, Department of Neurogenetics, Hermann-Rein-Strasse 3, D-37075Gottingen, Germany [2]Mitochondrial Research Group, Institute for Ageing and Health, The Medical School, Newcastle University, Framlington Place, Newcastle upon Tyne NE2 4HH, UK. [3]Biomedizinische NMR Forschungs GmbH am Max Planck Institute of Biophysical Chemistry, D-37070 Gottingen, Germany. [4]University of Miami, Miller School of Medicine, Department of Neurology and Cell Biology& Anatomy, 1095NW 14th Terrace, Miami, Florida 33136, USA. [5]Department of Cell Biology, Erasmus MC, 3000 CA Rotterdam, Netherlands. [6]Institute of Cell Biology, Department of Biology, ETH Honggerberg, Schafmattstrasse 18, 8093 Zurich, Switzerland. [7]Department of Clinical Neurophysiology, University of Gottingen (UMG), Robert-Koch-Strasse 40, D-37075 Gottingen, Germany.

Abstract

Oligodendrocytes, the myelin-forming glial cells of the central nervous system, maintain long-term axonal integrity[1–3]. However, the underlying support mechanisms are not understood[4]. Here we identify ametabolic component of axon–glia interactions by generating conditional Cox10 (protoheme IX farnesyltransferase) mutant mice, in which oligodendrocytes and Schwann cells fail to assemble stable mitochondrial cytochrome c oxidase (COX, also known as mitochondrial complex IV). In the peripheral nervous system, Cox10 conditional mutants exhibit severe neuropathy with dysmyelination, abnormal Remak bundles, muscle atrophy and paralysis. Notably, perturbing mitochondrial respiration did not cause glial cell death. In the adult central nervous system, we found no signs of demyelination, axonal degeneration or secondary inflammation. Unlike cultured oligodendrocytes, which are sensitive to COX inhibitors[5], post-myelination oligodendrocytes survive well in the absence of COX activity. More importantly, by in vivo magnetic resonance spectroscopy, brain lactate concentrations inmutants were increased compared with controls, but were detectable only in mice exposed to volatile anaesthetics. This indicates that aerobic glycolysis products derived from oligodendrocytes are rapidly metabolized within white matter tracts. Becausemyelinated axons can use lactate when energy-deprived[6], our findings suggest a model in which axon– glia metabolic coupling serves a physiological function.

The nuclear *Cox10* gene encodes a haem A farnesyl transferase, essential for the assembly of COX, the terminal complex of the electron transport chain in mitochondria[7, 8]. In COX10 mutants, COX is unstable and rapidly degraded. *Cox10flox/flox* mice have been used to generate models of severe mitochondrial disease in muscle, brain and liver[7, 8, 9, 10]. We crossed the *Cox10flox/flox* line[7] with *Cnp1Cre/+* mice[2] that express Cre recombinase in Schwann cells and oligodendrocytes (with Cre expression beginning at the respective precursor stages in these cells)[11, 12]. In the absence of functional COX, glial cells should fail to fully metabolize glucose, and should generate ATP mostly by glycolysis and produce lactate. Thus, demyelination and glial cell death would be key indicators for metabolic demands of glial cells, toxic effects of lactic acidosis, and metabolic coupling between neuronal and glial compartments in myelinated fibre tracts.

Crosses of *Cox10flox/+*Cnp1Cre/+* and *Cox10flox/flox*Cnp1+/+* mice led to fewer mutant pups (*Cox10flox/flox*Cnp1Cre/+*) than expected (11% compared with 25% expected, $n = 466$), suggesting prenatal death of some mice, probably owing to the known *Cnp1Cre/+* expression in a subset of neural precursors (see later). We therefore generated other mutants by selectively targeting Schwann cells (using *Dhh-Cre* mice) and mature oligodendrocytes (using tamoxifen-inducible *Plp1-CreERT2* mice), and found no evidence of embryonic lethality. In the following, data are from *Cnp1Cre/+*Cox10flox/flox* mutants (and *Cnp1Cre/+*Cox10flox/+* controls), unless otherwise stated.

Quantitative polymerase chain reaction (qPCR) of genomic DNA from neural tissue (at postnatal day (P) 21) confirmed the loss of exon 6 and thus a functional *Cox10* gene (Fig. 1a, b). For the sciatic nerve we calculated that $67 \pm 2\%$ (mean ± s.e.m., $n = 4$) of all cells were recombinant (assuming that both alleles recombine). Thus, most Schwann cells in peripheral nerves were successfully targeted. In the optic nerve and cervical spinal cord, we calculated that about 50% of cells were recombined at the *Cox10* locus (Fig. 1b), the estimated percentage of oligodendrocytes[13].

Elimination of *Cox10* is not immediately followed by the loss of respiration, but predicts the rapid functional 'ageing' of mitochondria, as the mitochondrial half-life is about 3 weeks in the brain[14, 15]. Thus, postnatal myelination by oligodendrocytes will involve intact mitochondria (Fig. 1c). By contrast, recombination of *Cox10* in proliferating Schwann cells causes a more rapid 'loss' of intact mitochondria by dilution in the progeny (Fig. 1c, right). Indeed, the absence of COX from many Schwann cells was obvious at P21 (Fig. 1d). For comparison, immunostaining of axonal mitochondria was indistinguishable between mutants and controls. We also noted occasional spinal motor neurons lacking COX (not shown), a plausible contributor to embryonic lethality.

A severe neuropathy phenotype proved that gene targeting was efficient and disruptive for mitochondrial function. Both *Cnp1Cre/+*Cox10flox/flox* and *Dhh-Cre*Cox10flox/flox* mice exhibited a developmental defect, with reduced weight, tremors and hindlimb weakness, although mutants appeared otherwise healthy and well groomed. The disease progressed to hindlimb paralysis and muscle atrophy (Supplementary Fig. 1a), followed by forelimb paralysis at about 9 months, when mutants had to be euthanized.

Already at P21 attempts to compare sciatic nerve conduction velocities between controls (15.6 ± 0.7 m s^{-1}; mean ± s.e.m.; $n = 5$) and mutant mice ($n = 5$) failed, indicating conduction blocks (Fig. 2a). Only distal stimulation elicited a compound muscle action potential in mutant mice, but with 50% reduced amplitude (Supplementary Fig. 1b), indicating a combination of glial and axonal perturbations. The same functional blocks were seen in *Dhh-Cre*Cox10flox/flox* mice (not shown), confirming the specificity for Schwann cells.

By morphology and TdT-mediated dUTP nick end labelling (TUNEL) staining, we found no evidence for Schwann cell death as a possible cause of hypomyelination (not shown). In fact, the number of cell nuclei was increased (Fig. 2b). Compared with controls, mutant nerves were thinner (Fig. 2c), the absolute number of myelinated axons was reduced (Fig. 2d) and many medium-sized axons remained unmyelinated (Supplementary Fig. 1c, d). However, neither large nor small axons were significantly altered in number (Supplementary Fig. 2a), suggesting a primary dysmyelination at P21. By immunostaining for the activated monocyte/macrophage marker MAC3, reactive macrophages were found to not yet be a feature (not shown), confirming the developmental defect. At later stages, the number of myelinated axons was reduced (Fig. 2d), and in 2-month-old mice fibre degeneration was already associated with secondary inflammation (Supplementary Fig. 2b). Notably, even at 9 months there was no major loss of Schwann cells, with 193 ± 25 per sciatic nerve section in mutants and 239 ± 17 in controls (mean $\pm$ s.e.m., $n = 4$).

Where myelin was present, g-ratio analysis (the ratio between the diameter of the inner axon and the total outer diameter) showed a decrease in myelin thickness (0.589 ± 0.009 in controls; 0.612 ± 0.012 in mutants; mean $\pm$ s.d., $n = 3$). By electron microscopy, many axons that appeared correctly sorted remained unmyelinated, despite a calibre $>1.0 \mu m$ (Fig. 2e–g). Remak cells failed to engulf single axons with cellular processes (Fig. 2f). Thus, the axonal sorting defect in mice lacking the transcription factor TFAM1 (ref. 16) is probably the consequence of perturbed COX activity in Schwann cells.

Mitochondria were visibly enlarged in mutant Schwann cells (Fig. 2h, i), but not in associated axons (Supplementary Fig. 2c), reflecting a loss of the proton gradient and a failure of H^+/K^+ antiporters[17]. Compacted myelin, when present, had a normal ultrastructure and was stable (Fig. 2h, i).

An intriguing aspect of altered energy metabolism in peripheral nerves was the increase of vascularization. Blood vessels covered a threefold larger area in cross-sections from mutant nerves (Supplementary Fig. 3a–c). Hypervascularization was associated with upregulation of *Vegfa* messenger RNA, but not of *Hif1a* or glucose transporters (Supplementary Fig. 3d), and is possibly a response to enhanced glycolysis.

Myelinated tracts were normally developed in brains and spinal cords of mice at 2 months of age (Supplementary Fig. 4), which is best explained by sufficient respiration of oligodendroglial mitochondria during myelination (Fig. 1c). The fact that losing mitochondrial function requires several weeks was confirmed by inactivating *Cox10* in postmitotic neurons (at P5–P10) using *CamKII-Cre* mice. As previously shown[10], these mice die prematurely with severe neurodegeneration, visualized by neuroinflammation and loss of hippocampal neurons at 4 months of age (Supplementary Fig. 5).

Surprisingly, even at 9 months of age when *Cnp1^{Cre/+}*Cox10^{flox/flox}* mice had to be killed because of peripheral neuropathy, we detected no signs of white matter pathology, demyelination or oligodendroglial pathology (Fig. 3a–f), although the absence of COX activity from oligodendrocyte lineage cells was obvious by sequential COX and succinate dehydrogenase (SDH, also known as mitochondrial complex II) histochemistry (Fig. 3g and Supplementary Fig. 6). Mature oligodendrocytes (CC1^+) instead showed an abnormal (SDH^+) mitochondrial expansion, but were COX^− (Fig. 3h). To extend the observational time window, we induced recombination by tamoxifen in *Plp1-CreERT2*Cox10^{flox/flox}* 1-month-old mice. Histological analysis at age 14 months (the latest time-point tested) also failed to show any signs of demyelination or neurodegeneration (Supplementary Fig. 7a–c). Furthermore, magnetic resonance imaging (MRI) showed that there was no difference in

ventricular volume between mutants (8.1 ± 1.1 mm^3 (mean ± s.d.)) and controls (8.4 ± 1.4 mm^3) at 6–7 months of age (Supplementary Fig. 7d, e).

Theoretically, white matter integrity could be preserved when mutant oligodendrocytes are replaced by newly generated oligodendrocytes that remyelinate. These cells might again survive for several weeks after recombination of *Cox10*. We think this is unlikely for several reasons. By electron microscopy and *g*-ratio analysis, central nervous system (CNS) myelin thickness in adult mutants was in the normal range (Fig. 3c, d and Supplementary Fig. 8), unlike remyelinated axons that are hypomyelinated[18]. Moreover, we failed to observe apoptotic cells in the white matter tracts of adult*Cox10* mutants (Supplementary Fig. 9a), and the administration of BrdU did not label more oligodendrocyte precursor cells in mutants than in age-matched controls (Supplementary Fig. 9b). Furthermore, staining for astrocytes, microglia and T cells (Supplementary Fig. 10) gave no indication of low-grade inflammation, a very sensitive response to degenerative processes in white matter tracts. We conclude that once myelination has occurred, reduced mitochondrial functions do not perturb oligodendrocyte survival, myelin maintenance or axonal integrity.

We proposed that oligodendrocytes survive by enhanced glycolysis, and predicted to see *in vivo* an increase in the brain lactate concentration using localized proton magnetic resonance spectroscopy (MRS). As expected, *Cox10* mutants showed a more strongly increased lactate resonance (compared with controls) in both cortex and white matter. Notably, accumulated brain lactate was detectable only under isoflurane anaesthesia (Fig. 4a). When quantified in adult mutants (Fig. 4b), we determined >4 mM lactate in the cortex and >6 mM in the corpus callosum (compared with <2 mM lactate in the cortex and <4 mM in the white matter of wild-type mice). At the end of anaesthesia, these lactate concentrations fell within minutes to very low levels (Fig. 4c). The latter finding is compatible with a model in which oligodendroglial release of lactate — the necessary by-product of aerobic glycolysis — is followed by its rapid use in other cellular compartments. It is demonstrated *in vitro* that glial lactate is efficiently metabolized by myelinated axons (Supplementary Fig. 11). *In vivo*, lactate levels never reached MRS detectability under physiological conditions, unless challenged by isoflurane anaesthesia. Of note, the levels of *N*-acetylaspartate (a marker of viable neurons and axons), choline-containing compounds (indicators of membrane turnover) and myo-inositol (an osmolyte and glial membrane constituent) further support our conclusion that neurodegeneration and abnormal oligodendrocyte turnover are not a feature (Supplementary Fig. 12).

COX10-deficient cells in culture are practically respiration-deficient[19]. Because we combined well-established lines of floxed mice and Cre transgenic tools, the reported phenotype is probably caused by the loss of mitochondrial ATP generation. In the periphery, the mitotic expansion of (mutant) Schwann cell precursors rapidly dilutes functional mitochondria, and hypomyelination demonstrates that myelination is an energy-consuming process. We also note that many patients with mitochondrial disorders have signs of neuropathy with hypomyelination. By contrast, unperturbed CNS myelination is best explained by sufficient residual function of mitochondria in mature oligodendrocytes after recombination (Fig. 1c). We note that germline mutations of human*COX10* and other COX assembly factors, although ultimately lethal, have been associated with CNS dysmyelination (leukodystrophy)[8].

Most intriguing is the mild post-myelination CNS phenotype of adult *Cox10* mutant mice, in which oligodendrocytes maintain myelin and their ensheathed axons. That mature oligodendrocytes apparently survive by aerobic glycolysis similar to tumour cells (known as the Warburg effect) was unexpected. In fact, oligodendrocytes *in vitro* are sensitive to the COX inhibitor azide[5]. However, these cells correspond to 'pre-myelinating'

oligodendrocytes *in vivo*, and it seems that metabolic properties of oligodendrocyte lineage cells change during maturation. After myelination, oligodendrocytes may tolerate a partly glycolytic metabolism that we have experimentally augmented in *Cox10* mutants. We note that mature wild-type oligodendrocytes have lower COX activity than oligodendrocyte precursor cells (not shown), and that white matter has relatively high glycolytic activity[20]. Also, in our control mice absolute lactate levels (as a surrogate marker for aerobic glycolysis) were higher in white than grey matter (Fig. 4b).

Enhanced glycolysis in oligodendrocytes increases the production of pyruvate, lactate and acetyl-coenzyme A (CoA), the latter promoting fatty acid synthesis during myelination. Because energy-deprived myelinated axons can rapidly use pyruvate and lactate as an alternative energy source[6,21] (Supplementary Fig. 11), we suggest a model in which an increased rate of oligodendroglial glycolysis can supply glycolysis products to support axonal energy needs (Fig. 4d).

Our observation that lactate levels in mutant brains are visibly increased compared with controls, but only under isoflurane anaesthesia, suggests that lactate is not cleared by drainage, but is locally metabolized. Isoflurane anaesthesia does not decrease CNS blood flow. The theoretical possibility that increased lactate peaks are caused by mutant oligodendrocytes that fail to metabolize neuronal lactate seems remote (note the similar lactate increases in grey matter, where neurons are associated with respiration-competent astrocytes[22]). Increased lactate concentrations probably originate from *Cox10* mutant oligodendrocytes that rely on increased glycolysis for survival. Even under normal conditions, lactate exported from oligodendrocytes would be rapidly metabolized and therefore not be detected by MRS.

By *in situ* hybridization[23] and immunoelectron microscopy[24], the monocarboxylate transporter MCT1 (also known as SLC16A1) is expressed in white matter, and is even present in myelin[24], whereas MCT2 localizes to myelinated axons. This strongly suggests that lactate generated in oligodendrocytes is released and reaches the axonal compartment (Fig. 4d).

We assume that oligodendrocytes can oxidize glycolysis-derived $NADH^+$ when mitochondria are intact (using a NADH-glycerolphosphate shuttle that is oligodendrocyte-specific[25]). Thus, normal oligodendrocytes may not even reduce pyruvate, which passes equally well through MCT1 and MCT2. Such a model of oligodendrocytes, yielding glycolysis products to axons when energy deprived[4], does not contradict the presumed role of lactate in the support of myelination during development[24], that is, when the import of metabolites is rate-limiting for lipid synthesis[26], specifically for oligodendrocytes in culture[24].

Our model of axon–oligodendrocyte metabolic coupling is reminiscent of the astroglial 'lactate shuttle', which is thought to support the energy metabolism of glutamatergic synapses in the cortex[27, 28]. For oligodendrocyte lineage cells, the inferred developmental 'switch' of metabolism even allows them to survive by aerobic glycolysis. The underlying mechanisms deserve further attention, as they may be relevant for the survival of glioma cells and the Warburg effect.

Methods

Animals

All animal experiments were carried out in compliance with animal policies of the State of Lower Saxony, Germany. Animals were maintained on a C57/Bl6 genetic background.

Cox10$^{flox/flox}$ mice[7],*Cnp1$^{Cre/+}$* mice[2], *Dhh-Cre* mice[29], *Plp1-CreERT2* mice[30] and *CamKII-Cre*[31] mice were genotyped as described. Tamoxifen treatment[30] was for 5 days, daily.

qPCR of genomic DNA

qPCR was performed using 10 ng of genomic DNA in a 12.5-μl assay using PowerSYBR Green PCR Master Mix (Applied Biosystems) on an Applied Biosystems 7500 Fast Real Time PCR system in triplicates. A standard curve was generated using genomic DNA from *Cox10$^{flox/flox}$*, *Cox10$^{flox/+}$* and*Cox10$^{+/+}$* animals. The values were standardized to an independent genomic marker. A 167-base-pair *Cox10^{flox}*-specific fragment was obtained with primers 5′-CGGGGATCAATTCGAGCTCGCC-3′ and 5′-CACTGACGCAGCGCCAGCATCTT-3′. The percentage of *Cox10* recombination was calculated by assuming that recombination affects both floxed alleles in Cre-expressing cells.

Quantitative PCR after reverse transcription

RNA was prepared in TRIzol (Invitrogen), followed by purification on a Qiagen RNeasy column. Complementary DNA was synthesized from 0.5 μg of total RNA using SuperscriptIII (Invitrogen) with random nonamer primers. qPCRs were run with PowerSYBR Green PCR Master Mix (Applied Biosystems) on an Applied Biosystems 7500 Fast real-time PCR system in quadruplicates (outliers were removed). The following primers were used: *Gapdh*, 5′-CAATGAATACGGCTACAGCAAC-3′ and 5′-TTACTCCTTGGAGGCCATGT-3′; *Glut-1* (also known as *Slc2a1*), 5′-ATGGATCCCAGCAGCAAG-3′ and 5′-CCAGTGTTATAGCCGAACTGC-3′; *Glut-3* (*Slc2a3*), 5′-CTGGACCTCCAACTTTCTGG-3′ and 5′-GCAGCGAAGATGATAAAAACG-3′; *Hif1a*, 5′-CATGATGGCTCCCTTTTTCA-3′ and 5′-GTCACCTGGTTGCTGCAATA-3′; *Vegfa*, 5′-TTACTGCTGTACCTCCACC-3′ and 5′-ACAGGACGGCTTGAAGAT-3′; 18S RNA: 5′-AAATCAGTTATGGTTCCTTTGGTC-3′ and 5′-GCTCTAGAATTACCACAGTTATCCAA-3′.

Electrophysiology

Mice were anaesthetized with xylacin and ketamin intraperitoneally. Two recording electrodes were inserted into the intrinsic foot muscle. Distal stimulation electrodes were inserted at the ankle. The proximal stimulation electrodes were inserted at the sciatic notch. Compound muscle action potentials (CMAPs) were recorded with a Jaeger-Toennies Neuroscreen instrument. Nerve conduction velocities were calculated from the distance between proximal and distal stimulation electrodes and the latency difference between the CMAPs after successive proximal and distal stimulation. CMAP amplitudes were calculated peak to peak.

Optic nerve recordings and oxygen glucose deprivation

Optic nerves from 2-month-old wild-type mice were gently removed and directly transferred into an interface perfusion chamber (Haas Top, Harvard Apparatus) and superfused with artificial cerebrospinal fluid (ACSF) containing: 124 mM NaCl, 3 mM KCl, 2 mM CaCl$_2$, 2 mM MgSO$_4$, 1.25 mM NaH$_2$PO$_4$, 23 mM NaHCO$_3$ and 10 mM glucose. The perfusion chamber was continuously aerated by a humidified mixture of 95% O$_2$ and 5% CO$_2$, and experiments were performed at 37 °C. Custom-made suction electrodes, back-filled with ACSF, were used for stimulation and recording. Compound action potentials (CAP) were evoked every 30 s with a square-wave (50 μs, 0.8 mA) constant current stimulus pulse (Stimulus Isolator 385, WPI). The recording electrode was connected to a Heka amplifier (EPC9), and the signal was amplified 500 times, filtered at 30 kHz, and acquired at 20–30

kHz. Before recording, optic nerves were equilibrated for at least 15 min in the chamber. After 1-h baseline recordings, optic nerves were exposed to oxygen glucose deprivation (OGD) for 1 h. OGD was induced by switching to glucose-free ACSF and a gas mixture containing 95% N_2 and 5% CO_2 in the recording chamber. To ensure that no oxygen was delivered by the superfusate, ACSF was always bubbled with 95% N_2, 5% CO_2. After OGD, control ACSF and O_2 were restored and CAPs were recorded for up to 2 h. To test the role of pyruvate and lactate transporters on energetic recovery, 200 μM α-cyano-4-hydroxycinnamic acid (Sigma Aldrich) was applied 20 min before recovery (for 40 min). Optic nerve function was monitored over time, as the area under the CAP that was normalized to baseline. Data are presented as mean ± s.e.m., with *n* indicating the number of optic nerves used in these experiments.

Serial COX and SDH histochemistry

Cryostat sections (8-μm thickness) were air-dried for 30 min before the application of COX medium (500 μM cytochrome *c*, 5 mM diaminobenzidine tetrahydrochloride and 20 mg ml^{-1} catalase). After incubation in COX medium at 37 °C for 40 min, the sections were washed three times using PBS and SDH medium (130 mM sodium succinate, 200 mM phenazine methosulphate, 1 mM sodium azide, 1.5 mM nitroblue tetrazolium in 0.1 M phosphate buffer, pH 7.0) was applied for 30 min at 37 °C.

Histology and immunohistochemistry

Animals were anaesthetized with avertin and perfused intracardially with 15 ml of HBSS, followed by 50 ml of fixative (4% formalin in phosphate buffer). Dissected nerves were postfixed overnight in fixative and embedded in paraffin. Gallyas' silver impregnation was performed as described[2]. Tissues for cryosections were dissected fresh, and snap-frozen or immersion-fixed for 1 h in fixative, infiltrated with 20% sucrose in PBS, and frozen in Shandon Cryomatrix. Antibodies used were mouse-anti-COX subunit-I (MitoSciences), rat-anti-CD31 (BD Pharmingen), anti-GFAP (Chemicon), anti-MAC3 (BD Pharmingen) and anti-CD3 (Serotec). Images were processed in Adobe Photoshop to equalize the contrast, and the background around semithin sections was manually cleared.

For immunofluorescent labelling of OLIG2 after COX and SDH histochemistry, the sections were fixed in cold 4% paraformaldehyde solution for 30 min and antigen retrieval was performed using boiling EDTA buffer, pH 8, for 1 min. Sections were washed in TBS three times for 5 min. Non-specific binding was blocked using 1% normal goat serum (Sigma) diluted in TBS. Sections were then incubated with primary antibody (OLIG2, rabbit immunoglobulin-G (IgG); Chemicon) overnight at 4 °C and detected using rhodamine-conjugated anti-rabbit secondary antibody (Jackson Immunoresearch). Sections were mounted using aqueous medium.

For double-labelling mitochondria in mature oligodendrocytes, we used COX-I (isotype IgG2a) and SDH (IgG1) antibodies from Mitosciences, and CC1 (IgG2b) antibodies from Calbiochem. Cryostat sections were air-dried for 30 min and fixed in cold 4% paraformaldehyde for 30 min. Gentle antigen retrieval was performed by immersing the section in boiling EDTA buffer, pH 7.4, for 30 s. After blocking in 1% normal goat serum, primary antibodies (1:200 for SDH 70 kDa and COX-I, and 1:100 for CC1) were applied for 90 min at room temperature. Indirect detection was with directly conjugated Alexia Fluor secondary antibodies (30 min at room temperature), and sections were mounted in Vector shield.

The TUNEL assay was performed using DeadEndTM Colorimetric TUNEL System kit following the manufacturer's protocol (Promega). For labelling mitotic cells, BrdU (100 μg

g^{-1}) was injected (intraperitoneally) at 4 months of age (for 4 weeks at 5 days a week). Brains were embedded in paraffin and sections (5 µm) were stained with anti-BrdU (Chemicon) and anti-OLIG2 antibodies (a gift from from C. Stiles).

Semithin sections and electron microscopy

Animals were anaesthetized with avertin and perfused intracardially with 15 ml of HBSS, followed by 50 ml of fixative (2.5% glutaraldehyde, 4% paraformaldehyde in PBS). Dissected nerves were postfixed overnight in fixative and embedded in Epon. Semithin sections were stained with methylene blue and AzurII. Ultrathin sections were contrasted with 1% uranyl acetate and lead citrate. Electron microscopic pictures were taken on a LEO 912AB electron microscope (Zeiss) with an on-axis 2048 × 2048 charge coupled device camera (Proscan). All cell counts and tracings were done using ImageJ (http://rsb.info.nih.gov/ij/). For semithin sections, entire cross-sections of sciatic nerves were scored. Optic nerves were freshly isolated and cryofixed by high-pressure freezing and freeze substituted. On electron microscopic pictures, all axons in three random fields (5,500 µm^2 total) per nerve were traced. The *g*-ratios were calculated from circular areas equal to the measured area of the fibres.

MRI and MRS

MRI and MRS was performed as recently described[32] on mutant and controls (*Cox10$^{flox/+}$*Cnp1$^{Cre/+}$*) at 4–5 months (*n* = 6/6) and 6–7 months (*n* = 7/7). Mice were initially anaesthetized with 5% isoflurane, subsequently intubated and kept under anaesthesia with 1.75% isoflurane in ambient air. In four mice, further spectra were obtained without anaesthesia. In these mice, pancuronium (15 mg kg^{-1}) was administrated 15 min before switching off the isoflurane supply to avoid movement artefacts. *In vivo* localized proton MRS (STEAM, TR/TE/TM = 6,000/10/10 ms) in different regions of the brain (cortex 3.9 × 0.7 × 3.2 mm^3, corpus callosum 2.5 × 1.0 × 2.0 mm^3, striatum 1.2 × 1.4 × 2.0 mm^3, cerebrum 4 × 3 × 4 mm^3) was performed at 9.4 T (Bruker Biospin GmbH). T2-weighted MRI (2D FSE, TR/TE = 4,200/43 ms, 8 echoes, resolution 100 × 100 µm^2, slice thickness 300 µm) in axial and horizontal orientation served to ensure a proper position of volumes-of-interest. These images were further used to measure the ventricular volume by manual segmentation (Amira Software, Visage Imaging, Berlin, Germany). Metabolite quantification involved spectral evaluation by LCModel[33] and calibration with brain water concentration. Metabolites with Cramer-Rao lower bounds above 20% were excluded from further analyses unless noted otherwise.

References

1. Griffiths I, et al. Axonal swellings and degeneration in mice lacking the major proteolipid of myelin. Science. 1998; 280:1610–1613. [PubMed: 9616125]

2. Lappe-Siefke C, et al. Disruption of *Cnp1* uncouples oligodendroglial functions in axonal support and myelination. Nature Genet. 2003; 33:366–374. [PubMed: 12590258]

3. Kassmann CM, et al. Axonal loss and neuroinflammation caused by peroxisome-deficient oligodendrocytes. Nature Genet. 2007; 39:969–976. [PubMed: 17643102]

4. Nave KA. Myelination and the trophic support of long axons. Nature Rev. Neurosci. 2010; 11:275–283. [PubMed: 20216548]

5. Ziabreva I, et al. Injury and differentiation following inhibition of mitochondrial respiratory chain complex IV in rat oligodendrocytes. Glia. 2010; 58:1827–1837. [PubMed: 20665559]

6. Tekkök SB, Brown AM, Westenbroek R, Pellerin L, Ransom BR. Transfer of glycogen-derived lactate from astrocytes to axons via specific monocarboxylate transporters supports mouse optic nerve activity. J. Neurosci. Res. 2005; 81:644–652. [PubMed: 16015619]

7. Diaz F, Thomas CK, Garcia S, Hernandez D, Moraes CT. Mice lacking *COX10* in skeletal muscle recapitulate the phenotype of progressive mitochondrial myopathies associated with cytochrome *c* oxidase deficiency. Hum. Mol. Genet. 2005; 14:2737–2748. [PubMed: 16103131]

8. Antonicka H, et al. Mutations in *COX10* result in a defect in mitochondrial heme A biosynthesis and account for multiple, early-onset clinical phenotypes associated with isolated COX deficiency. Hum. Mol. Genet. 2003; 12:2693–2702. [PubMed: 12928484]

9. Diaz F, et al. Pathophysiology and fate of hepatocytes in a mouse model of mitochondrial hepatopathies. Gut. 2008; 57:232–242. [PubMed: 17951359]

10. Fukui H, Diaz F, Garcia S, Moraes CT. Cytochrome *c* oxidase deficiency in neurons decreases both oxidative stress and amyloid formation in a mouse model of Alzheimer's disease. Proc. Natl Acad. Sci. USA. 2007; 104:14163–14168. [PubMed: 17715058]

11. Goebbels S, et al. Elevated phosphatidylinositol 3,4,5-trisphosphate in glia triggers cell-autonomous membrane wrapping and myelination. J. Neurosci. 2010; 30:8953–8964. [PubMed: 20592216]

12. Genoud S, et al. Notch1 control of oligodendrocyte differentiation in the spinal cord. J. Cell Biol. 2002; 158:709–718. [PubMed: 12186854]

13. Miller RH, David S, Patel R, Abney ER, Raff MC. A quantitative immunohistochemical study of macroglial cell development in the rat optic nerve: *in vivo* evidence for two distinct astrocyte lineages. Dev. Biol. 1985; 111:35–41. [PubMed: 3896893]

14. Beattie DS, Basford RE, Koritz SB. The turnover of the protein components of mitochondria from rat liver, kidney, and brain. J. Biol. Chem. 1967; 242:4584–4586. [PubMed: 6061404]

15. Menzies RA, Gold PH. The turnover of mitochondria in a variety of tissues of young adult and aged rats. J. Biol. Chem. 1971; 246:2425–2429. [PubMed: 5553400]

16. Viader A, et al. Schwann cell mitochondrial metabolism supports long-term axonal survival and peripheral nerve function. J. Neurosci. 2011; 31:10128–10140. [PubMed: 21752989]

17. Garlid KD, Paucek P. Mitochondrial potassium transport: the K^+ cycle. Biochim. Biophys. Acta. 2003; 1606:23–41. [PubMed: 14507425]

18. Dubois-Dalcq M, Ffrench-Constant C, Franklin RJ. Enhancing central nervous system remyelination in multiple sclerosis. Neuron. 2005; 48:9–12. [PubMed: 16202704]

19. Diaz F, Fukui H, Garcia S, Moraes CT. Cytochrome *c* oxidase is required for the assembly/stability of respiratory complex I in mouse fibroblasts. Mol. Cell. Biol. 2006; 26:4872–4881. [PubMed: 16782876]

20. Moreland C, Henjum S, Iversen EG, Skredde KK, Hassel B. Evidence for a higher glycolytic than oxidative metabolic activity in white matter of rat brain. Neurochem. Int. 1990; 50:703–709.

21. Brown AM, Wender R, Ransom BR. Metabolic substrates other than glucose support axon function in central white matter. J. Neurosci. Res. 2001; 66:839–843. [PubMed: 11746409]

22. Gandhi GK, Cruz NF, Ball KK, Dienel GA. Astrocytes are poised for lactate trafficking and release from activated brain and for supply of glucose to neurons. J. Neurochem. 2009; 111:522–536. [PubMed: 19682206]

23. Vannucci SJ, Simpson IA. Developmental switch in brain nutrient transporter expression in the rat. Am. J. Physiol. Endocrinol. Metab. 2003; 285:E1127–E1134. [PubMed: 14534079]

24. Rinholm JE, et al. Regulation of oligodendrocyte development and myelination by glucose and lactate. J. Neurosci. 2011; 31:538–548. [PubMed: 21228163]

25. Leveille PJ, McGinnis JF, Maxwell DS, de Vellis J. Immunocytochemical localization of glycerol-3-phosphate dehydrogenase in rat oligodendrocytes. Brain Res. 1980; 196:287–305. [PubMed: 6772276]

26. Jalil MA, et al. Reduced *N*-acetylaspartate levels in mice lacking aralar, a brain- and muscle-type mitochondrial aspartate-glutamate carrier. J. Biol. Chem. 2005; 280:31333–31339. [PubMed: 15987682]

27. Pellerin L, Magistretti PJ. Glutamate uptake into astrocytes stimulates aerobic glycolysis: a mechanism coupling neuronal activity to glucose utilization. Proc. Natl Acad. Sci. USA. 1994; 91:10625–10629. [PubMed: 7938003]

28. Suzuki A, et al. Astrocyte-neuron lactate transport is required for long-term memory formation. Cell. 2011; 144:810–823. [PubMed: 21376239]

29. Jaegle M, et al. The POU proteins Brn-2 and Oct-6 share important functions in Schwann cell development. Genes Dev. 2003; 17:1380–1391. [PubMed: 12782656]

30. Leone DP, et al. Tamoxifen-inducible glia-specific Cre mice for somatic mutagenesis in oligodendrocytes and Schwann cells. Mol. Cell. Neurosci. 2003; 22:430–440. [PubMed: 12727441]

31. Minichiello L, et al. Essential role for TrkB receptors in hippocampus-mediated learning. Neuron. 1999; 24:401–414. [PubMed: 10571233]

32. Michaelis T, Boretius S, Frahm J. Localized proton MRS of animal brain *in vivo*: Models of human disorders. Prog. Nucl. Magn. Reson. Spectrosc. 2009; 55:1–34.

33. Provencher SW. Estimation of metabolite concentrations from localized in vivo proton NMR spectra. Magn. Reson. Med. 1993; 30:672–679. [PubMed: 8139448]
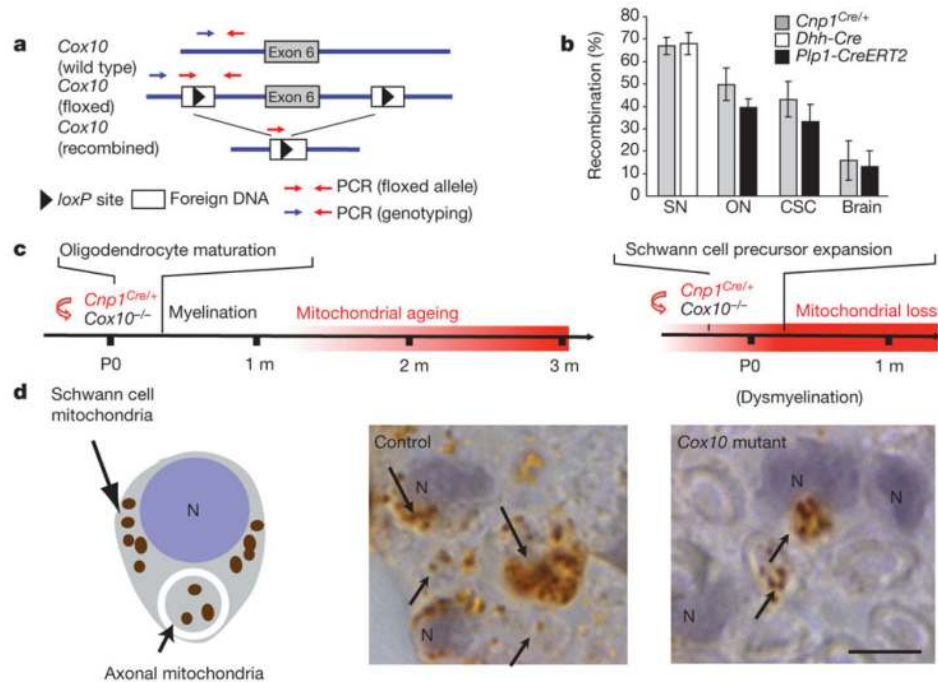
Figure 1. Genetic targeting of the mitochondrial COX complex in myelinating glial cells
a, Conditional mutagenesis of the floxed Cox10 gene, deleting exon 6 (not drawn to scale). Arrows indicate the location of primers for genotyping (blue/red) and qPCR (red/red), the latter amplifying only the floxed allele. **b**, Loss of the floxed Cox10 gene in myelinating glial cells of different Cre-expressing mice (adult), confirmed by qPCR of genomic DNA. Highest fraction of myelinating glia are found in sciatic nerve (SN), followed by optic nerve (ON), cervical spinal cord (CSC) and total brain. Mean percentages ± s.d. are shown; n = 3–5. **c**, Left panel, schematic time line showing that Cox10 genomic recombination in immature oligodendrocytes of newborn Cnp1[Cre/+] mice does not interfere with postnatal myelination. Mutant oligodendrocytes myelinate (first 3 weeks), using pre-existing mitochondria that will subsequently decline in respiratory function (marked 'ageing'). Right panel, for comparison, Cox10 recombination in proliferating Schwann cell precursors perturbs mitochondrial function before myelination, as intact mitochondria are 'lost' by dilution with mutant mitochondria. M, month. **d**, Right panels, myelinated axons and Schwann cells in motor roots of control and mutant animals at P21. The left panel shows a schematic representation. Cox10 mutant Schwann cells (but not axons) lose unstable COX, as demonstrated by reduced immunostaining for the catalytic COX subunit I (brown) in paraffin sections. Schwann cell nuclei (N) are counterstained in pale blue. Upward arrow, COX staining of axonal mitochondria; downward arrow, COX in Schwann cells. Scale bar, 10 μm.
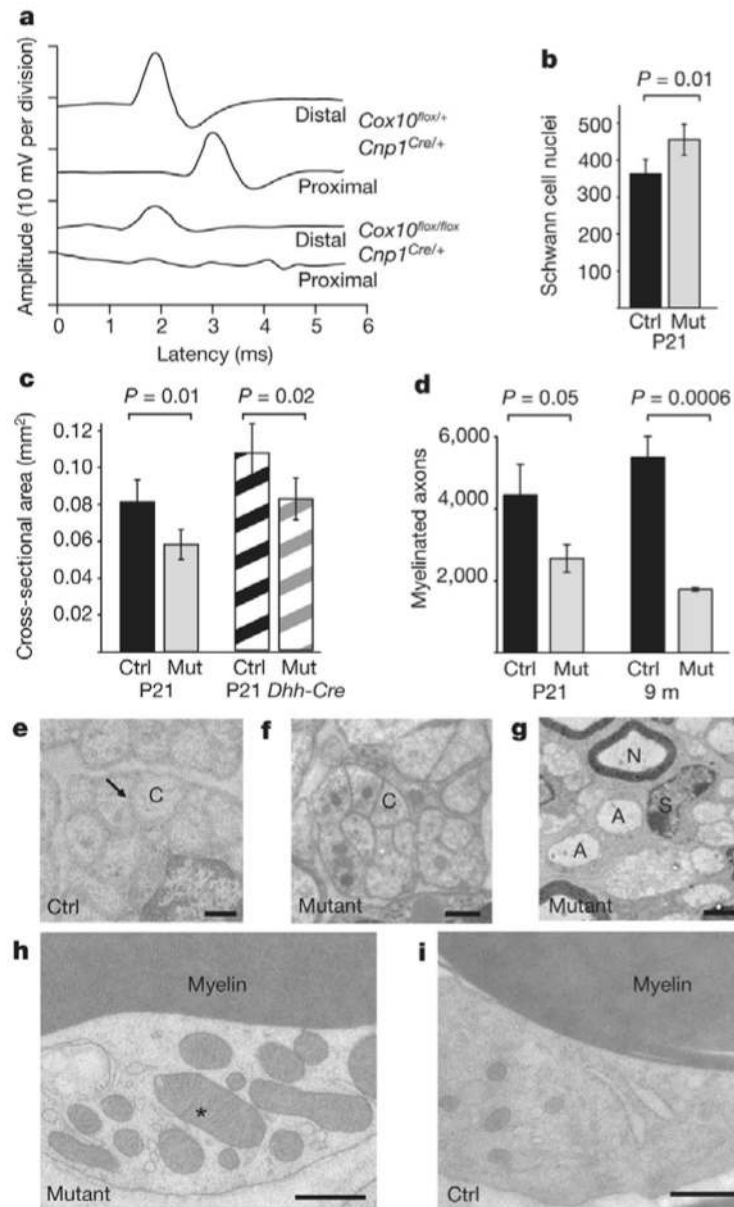
Figure 2. Peripheral neuropathy caused by *Cox10* mutant Schwann cells

a, Amplitudes of compound muscle action potentials were recorded in controls and mutant mice at P21 after proximal or distal stimulation of sciatic nerves, but were barely detectable in the mutants. **b–d**, The morphology of sciatic nerves was assessed in semithin sections, and the number of Schwann cell nuclei was counted (**b**), the cross-sectional area of the nerve with fascicles of axons and Schwann cells was determined (**c**), and the absolute number of myelinated axons counted (**d**). This showed a progressive loss of axons at older age, but not of Schwann cells. All data area mean ± s.d. Ctrl, control; mut, mutant. **e–i**, Electron microscopy showed differences between mutant and control sciatic nerves. **e**, **f**, In Remak bundles, C-fibre axons (C) are normally sorted by Schwann cell processes (**e**, arrow) but not in mutants (**f**).**g**, Mutant Schwann cells that fail to myelinate survive well. Note numerous unmyelinated medium-calibre axons (A) next to normally myelinated axons (N) and intact Schwann cell nuclei (S). **h**, **i**, At higher magnification, myelin appeared morphologically

normal, but mutant mitochondria (asterisk) were clearly enlarged. Scale bars, 500 nm (**e**, **f**, **h**, **i**), 2 μm (**g**).
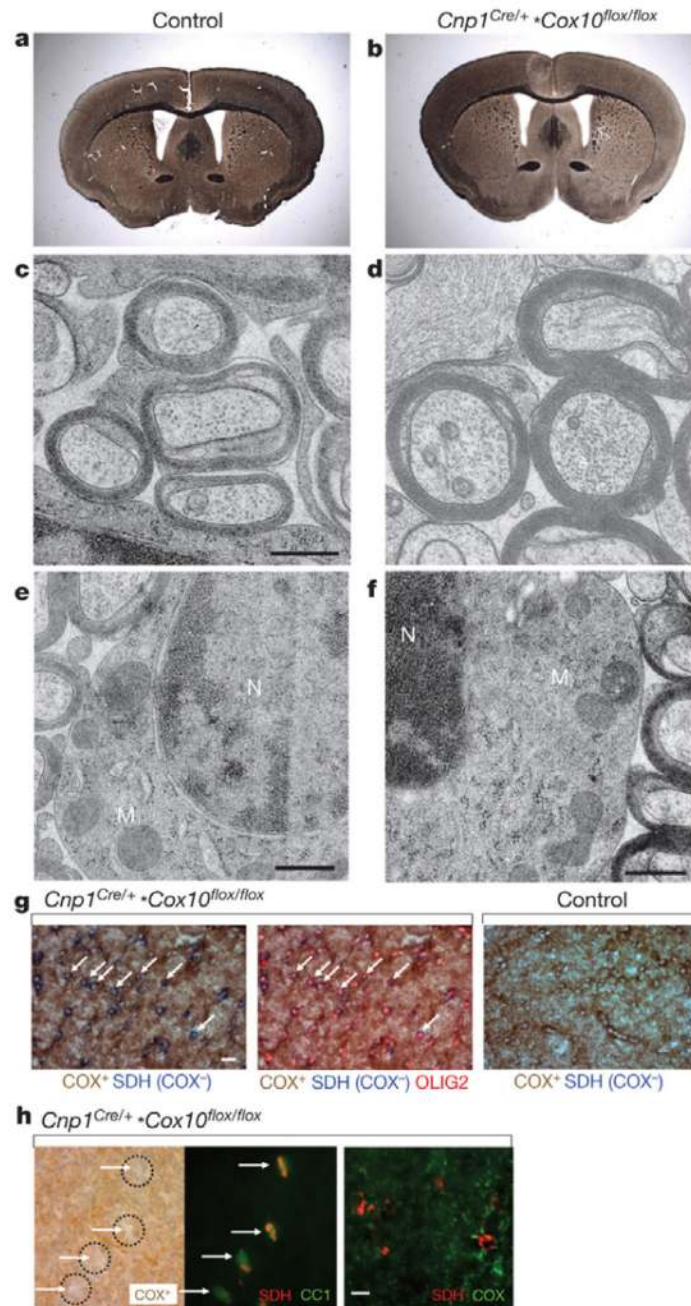
Figure 3. Oligodendroglial survival, myelin preservation and white matter integrity in *Cnp1*^Cre/+^*Cox10^flox/flox^ mice

a, **b**, By Gallyas' silver impregnation of myelin at 9 months of age, the corpus callosum and other white matter tracts appear normally developed and stable in mutant mice. **c–f**, Electron microscopy of high-pressure frozen optic nerve shows intact myelination of CNS axons (**c**, **d**), and healthy oligodendroglia nuclei (**e**, **f**). A, axon; N, nucleus; M, mitochondria. Scale bars, 0.5 µm. **g**, Serial COX and SDH histochemistry. Left, in the normal appearing white matter of 9-month-old Cnp1^Cre/+^*Cox10^flox/flox^ mutants (corpus callosum), mitochondrial COX activity yields a brown precipitate (axons and astrocytes, for example). By serial COX and SDH histochemistry, only Cox10-mutant COX⁻ cells are visibly stained for SDH (blue

precipitate, white arrows). Middle, about half (48.2 ± 6.5%) of the OLIG2-positive oligodendrocyte lineage cells in the mutant corpus callosum (red nuclei in overlay), that is, mostly mature oligodendrocytes that express CNP1[Cre], are lacking COX activity (blue). Right, there are no COX⁻ cells in the corpus callosum of age-matched controls. Scale bar, 20 μm. **h**, Left, when combining only COX histochemistry with a marker for mature cells (CC1), mutant oligodendrocytes (corpus callosum; 9 months of age) appear white (arrows), intermingled with COX⁺ neighbouring cells and compartments. Middle, mature oligodendrocytes that are CC1⁺ (green) are filled with abnormally large numbers of SDH⁺ mitochondria (red), and appear in orange in the overlay. Note the near absence of SDH signals from neighbouring cells and compartments. Right, in a separate overlay, the SDH⁺ mitochondria (red) are virtually devoid of COX immunostaining (green) in mutant oligodendrocytes. Scale bar, 10 μm.
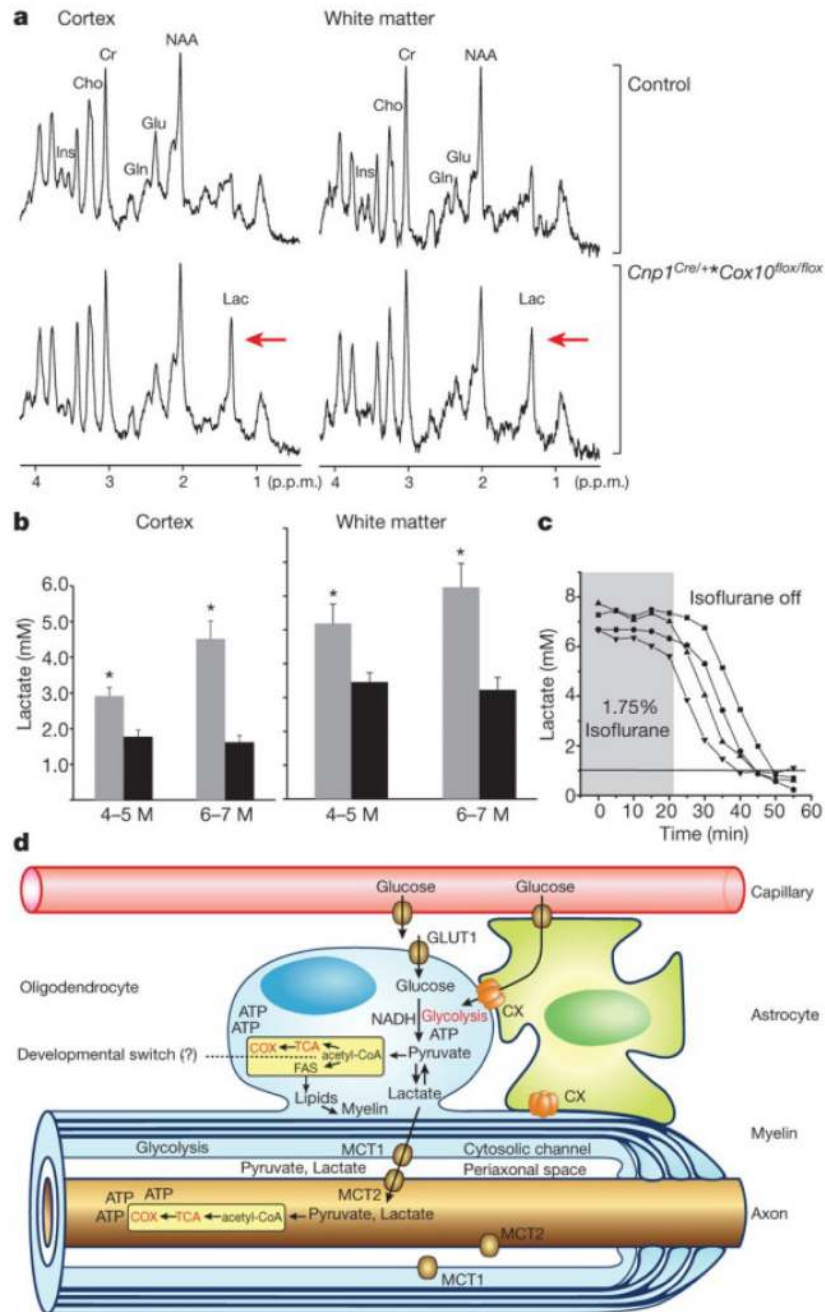
Figure 4. Rapid use of lactate shown by proton MRS

a, Localized proton magnetic resonance spectra of the cortex (left) and corpus callosum (right) fromCnp1$^{Cre/+}$∗Cox10$^{flox/flox}$ mutants and controls (6–7 months of age). Cr, total creatine; Ins, myo-inositol; p.p.m., parts per million; NAA, N-acetylaspartate. Red arrows denote lactate (Lac). **b**, Lactate levels in the cortex (left) and white matter (right) are increased in mutant mice (grey bars) compared with controls (black bars) under isoflurane anaesthesia. Data are mean ± s.e.m.; n = 6–7 per genotype. Note that under isoflurane anaesthesia the control mice have higher lactate levels in white matter than in grey matter. M, months. **c**, Increased brain lactate levels drop to undetectable levels in less than 60 min at

the end of isoflurane anaesthesia. This suggests that lactate (produced by oligodendrocytes) is rapidly metabolized by other cellular compartments in the white matter tracts of awake mice. **d**, Hypothetical model of metabolic coupling between oligodendrocytes and myelinated axons. Oligodendrocytes import glucose through GLUT1 (and possibly via astrocytes and gap junctions; CX, connexin) for glycolysis. Pyruvate is metabolised in mitochondria (yellow) for ATP generation (TCA, tricarboxylic acid cycle). With the onset of myelination ('developmental switch'), glucose also serves the synthesis of fatty acid (FAS) and myelin lipids from acetyl-CoA. In post-myelination oligodendrocytes, glycolysis can yield sufficient ATP to support oligodendrocyte survival. Glycolysis products are used by myelinated axons when energy levels are low[6,21]. Lactate (or pyruvate when NADH is oxidized in oligodendroglial mitochondria) can be directly transferred via monocarboxylic acid transporters (MCT1, MCT2), which reside in internodal myelin[24] and the axonal compartment, such that lactate is rapidly cleared in vivo (in **c**). Note that myelinated axons, largely shielded from the extracellular milieu[4], are separated by a thin periaxonal space from the oligodendroglial cytoplasm filling the inner loops of myelin ('cytosolic channel') and paranodal loops.